Development of the ion cyclotron emission diagnostic for the W7-X stellarator

D. Moseev, R. Ochoukov, V. Bobkov, R. O. Dendy, H. Faugel, D. Hartmann, J.-P. Kallmeyer, J. Lansky, H. P. Laqua, S. Marsen, K. G. McClements, S. K. Nielsen, A. Reintrog, M. Salewski, B. S. Schmidt, T. Schulz, T. Stange, and W7-X Team

COLLECTIONS

View Online · Export Citation · CrossMark

ARTICLES YOU MAY BE INTERESTED IN

Development of a narrow stopband filter for spectroscopic fast ion deuterium-alpha measurements
Review of Scientific Instruments **92**, 033107 (2021); https://doi.org/10.1063/5.0040589

Upgrades to the ion cyclotron emission diagnostic on the DIII-D tokamak
Review of Scientific Instruments **92**, 033543 (2021); https://doi.org/10.1063/5.0040597

Physics and applications of three-ion ICRF scenarios for fusion research
Physics of Plasmas **28**, 020501 (2021); https://doi.org/10.1063/5.0021818
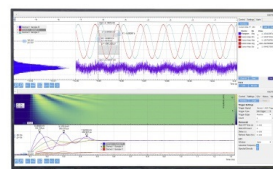
Development of the ion cyclotron emission diagnostic for the W7-X stellarator

View Online   Export Citation   CrossMark

D. Moseev,[1,a)] R. Ochoukov,[1] V. Bobkov,[1] R. O. Dendy,[2,3] H. Faugel,[1] D. Hartmann,[1] J.-P. Kallmeyer,[1]
J. Lansky,[4] H. P. Laqua,[1] S. Marsen,[1] K. G. McClements,[3] S. K. Nielsen,[5] A. Reintrog,[1] M. Salewski,[5]
B. S. Schmidt,[5] T. Schulz,[1] T. Stange,[1] and W7-X Team[1,b)]

AFFILIATIONS

[1] Max-Planck-Institut für Plasmaphysik, Greifswald, Garching, Germany
[2] Centre for Fusion, Space and Astrophysics, University of Warwick, Coventry CV4 7AL, United Kingdom
[3] Culham Centre for Fusion Energy, Culham Science Centre, Abingdon, Oxfordshire OX14 3DB, United Kingdom
[4] Hochschule Stralsund, Stralsund, Germany
[5] Department of Physics, Technical University of Denmark, Kgs., Lyngby, Denmark

Note: This paper is published as part of the Special Topic on Proceedings of the 23rd Topical Conference on High-Temperature Plasma Diagnostics.
a)Author to whom correspondence should be addressed: dmitry.moseev@ipp.mpg.de
b)See full W7-X Team list in T. Klinger *et al.*, Nucl. Fusion **59**, 112004 (2019).

ABSTRACT

An ion cyclotron emission (ICE) diagnostic is prepared for installation into the W7-X stellarator, with the aim to be operated in the 2022 experimental campaign. The design is based on the successful ICE diagnostic on the ASDEX Upgrade tokamak. The new diagnostic consists of four B-dot probes, mounted about 72° toroidally away (one module) from the neutral beam injector, with an unobstructed plasma view. Two of the B-dot probes are oriented parallel to the local magnetic field, aimed to detect fast magnetosonic waves. The remaining two probes are oriented poloidally, with the aim to detect slow waves. The radio frequency (RF) signals picked up by the probes are transferred via 50 Ω vacuum-compatible coaxial cables to RF detectors. Narrow band notch filters are used to protect the detectors from possible RF waves launched by the W7-X antenna. The signal will be sampled with a four-channel fast analog-to-digital converter with 14 bit depth and 1 GSample/s sampling rate. The diagnostic's phase–frequency characteristic is properly measured in order to allow measuring the wave vectors of the picked up waves.

I. INTRODUCTION

Ion cyclotron emission (ICE) is a radiative instability of the plasma in the ion cyclotron frequency range. The diagnostic is widely used in tokamaks for studying plasma instabilities that are mainly driven by fast ions, although the emission has been observed in thermal plasmas as well.[1] ICE is also often used as a qualitative indicator of the presence of fast ions in the plasma. Currently, efforts are made to turn the ICE diagnostic into a quantitative fast-ion diagnostic by constructing its weight functions,[2] as it is already done for other fast-ion diagnostics.[3–6] The applicability of the diagnostic to ITER has been studied.[7] The diagnostic is shown to be sensitive to fusion products in JET and TFTR,[8] DIII-D,[9] JT-60U,[10]

KSTAR,[11] ASDEX Upgrade,[12] and many others. The emission is often interpreted as magnetoacoustic cyclotron instability[13–18] and compressional Alfvén eigenmodes.[19,20]

ICE measurements were also reported from the large helical device.[21,22] In stellarators, fast-ion studies, in general, and ICE studies, in particular, are challenging because of the broken toroidal symmetry. The magnetic field topology changes with the toroidal angle, and it is difficult to relate a particular field strength to a certain radial position. Additionally, the fast-ion velocity distribution function is a function of toroidal angle as well.

The diagnostic for Wendelstein 7-X is based on the ICE diagnostic at ASDEX Upgrade, where it successfully measured fast-ion driven ICE[12,18,23,24] and compressional Alfvén

eigenmodes.[20] In Wendelstein 7-X, the diagnostic consists of four inductors measuring changes in the magnetic field in toroidal and poloidal directions for detecting fast magnetosonic waves and slow waves, respectively. The magnetic field in W7-X ranges between 2.1 and 2.8 T, depending on the position in the machine and magnetic configuration, which corresponds to the ion cyclotron frequency of hydrogen between 32 and 43 MHz. In contrast to ASDEX Upgrade, the neutral beam injector (NBI) system in W7-X generates sub-Alfvénic hydrogen fast ions with a full energy of 55 keV and with a maximum power of 1.7 MW.[25] The NBI power will be doubled in the coming campaign.

In this article, we describe the diagnostic to be prepared for the next operation phase of the stellarator, when the ion cyclotron resonant heating (ICRH) system and additional neutral beam injector (NBI) sources will be installed and describe attempts of measuring ICE in the previous campaign OP1.2, when the first two NBI sources were commissioned. We briefly describe the setup in the last campaign, when the design did not allow us measuring the signal, in Sec. II. The improved diagnostic setup for the next campaign is discussed in Sec. III. Section IV concludes this paper.

II. DESIGN OF THE ICE DIAGNOSTIC IN THE 2018 CAMPAIGN (OP1.2b)

In the previous experimental campaign in 2018 (OP1.2), first two sources of a neutral beam injector (NBI) were installed and commissioned in W7-X. Preliminary estimations based on the shape of the fast-ion velocity distribution function indicated that generation of ICE is possible. The plans for the diagnostic emerged already during the campaign. We adopted the same types of detectors as used on ASDEX Upgrade (SUMIDA inductors series 5120) and installed two

FIG. 1. A top-view schematic demonstrating the relative location of the ICE probes to the NBI and ECRH systems in W7-X. The ICE probes and the NBI sources are located in the neighboring modules, which are displaced 72° toroidally.

of them into the immersion tube for infrared cameras in the electron cyclotron resonance heating (ECRH) launchers in the bean-shaped cross section.[26] These ECRH launchers are located in toroidal module 1, while the NBI sources are in toroidal module 2. The modules are separated toroidally by 360°/5 = 72°, since W7-X has fivefold toroidal symmetry. One can see the location of ICE probes relative to the sources of fast ions in a top-view schematic in Fig. 1.

The characteristics of the detectors are reported.[27] The probes were connected to various radio frequency (RF) amplifiers that provided gain of 16.5–40 dB for frequencies up to 1 GHz and connected without amplifiers directly to an analog-to-digital converter (ADC). A four-channel analog-to-digital converter (ADC) ADQ14 from *SP Devices* with a sampling rate of 1.6 GSamples/s and analog bandwidth of 0.5 GHz was used.

The probe was located in the immersion tube with 50 mm inner diameter. The aperture to the plasma was 15 mm. Waves with a vacuum wavelength on the order of 10 m are, therefore, at cutoff: propagation requires that the size of the tube is not less than half a wavelength. The strength of the ICE signal was insufficient for the measurements in the evanescent region. Therefore, improvements in the design of the diagnostic are necessary; they are presented in Sec. III.

III. DESIGN OF THE ICE DIAGNOSTIC FOR THE FUTURE OPERATION CAMPAIGN (OP2)

In order to improve the measurements, the ICE detectors are placed at a new location. The new location should provide an unobstructed view for the probes into the plasma. The backside of a heat shield of the receiving antenna of the Collective Thomson Scattering (CTS) diagnostic[28] is chosen for mounting the detectors. The general scheme of the diagnostic is shown in Fig. 2. The magnetic probes are shielded from the plasma and stray microwave radiation by the heat shield and metallic housing. W7-X is a superconducting stellarator, and its plasma vessel is surrounded by a cryostat, where superconducting coils generate the magnetic field at a cryogenic temperature of 4 K. The distance between the plasma vessel and the cryostat wall is, depending on toroidal and poloidal locations, slightly less than 2 m. The plasma vessel ports are deep since they have to bridge over the cryovacuum in order to provide access to the plasma vessel from outside of the machine. Therefore, the ICE signal that we measure at the plasma vessel wall has to be transferred to the vacuum flange over a significant distance, as shown in Fig. 2. We use special Kapton-insulated vacuum-compatible 50 Ω coaxial cables inside actively cooled oxygen-free copper pipes to bridge over this gap. Four vacuum-compatible SMA (Sub-Miniature-A) feedthroughs with the PEEK (polyether ether ketone) insulator instead of conventional Teflon are used for transmitting the signals out of the vacuum vessel. Outside the vessel, we have matching units installed in order to provide best possible coupling of the signal into an ADC. Narrow notch filters for 37.5 MHz are installed before the ADC in order to protect it from the ion cyclotron resonance heating (ICRH) stray radiation. A four-channel 1 GSample/s ADC with an analog bandwidth of 400 MHz is used for digitization of the probe measurements. There will also be a possibility to use the ICRH antenna as a receiver and connect it to one of the ADC channels.
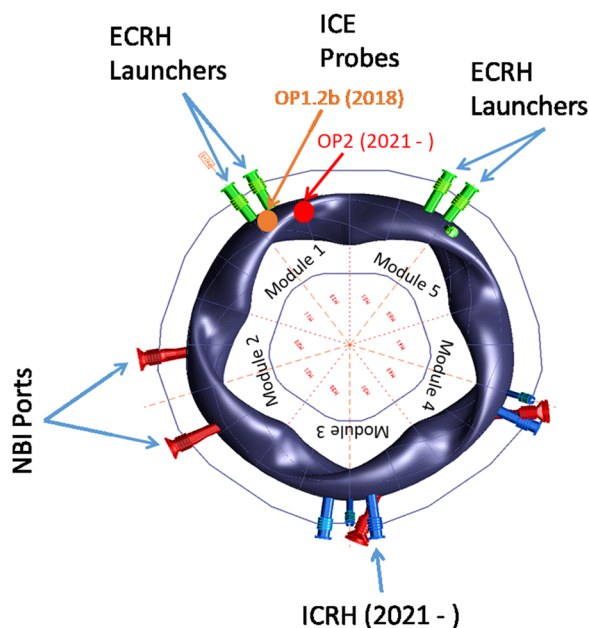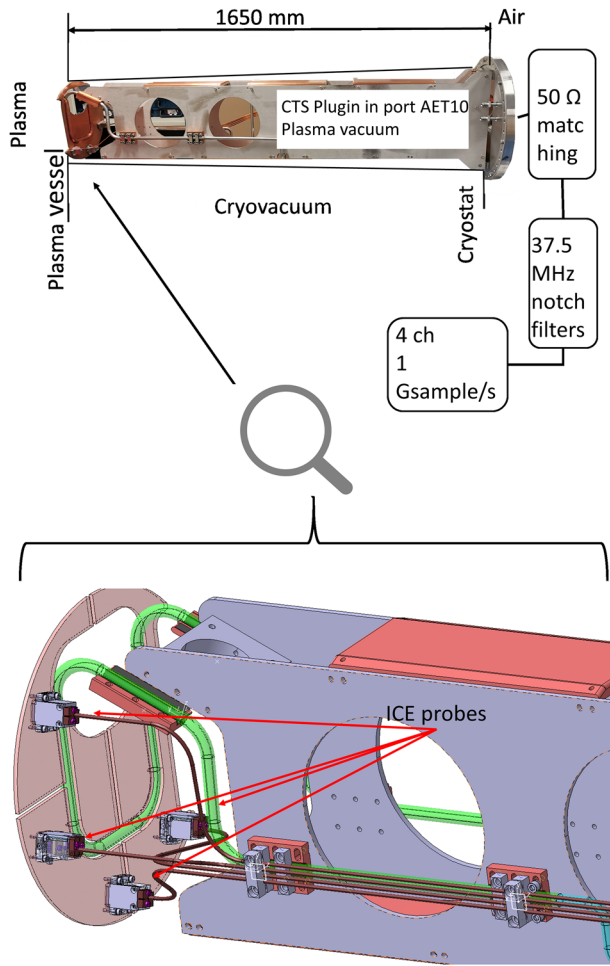
FIG. 2. A general schematic of a setup of the ICE diagnostic for OP2. In the upper panel, a poloidal cut of W7-X is sketched. The plasma is on the left side of the plasma vessel wall, and air is on the right from the cryostat. The AET10 port, where the CTS plugins with ICE detectors are installed, is a tube that connects the plasma vessel with an opening in the cryostat, bridging over cryovacuum. Matching elements, notch filters, and the ADC are installed outside the machine. The lower panel displays a zoomed-in view of the heat shield of the CTS plugin, where ICE probes are mounted.

From the upcoming experimental campaign onward, all in-vessel components of W7-X must be able to sustain a certain heat flux of plasma and stray radiation in the steady-state. One of the receiving antennas of the CTS diagnostic is installed in port AET10 in the direct proximity of electron cyclotron resonance heating (ECRH) launchers. It has to handle 100 kW/m^2 of radiation in the steady-state. In order to secure the diagnostic components, the antenna plug-in is equipped with an actively cooled stainless steel heat shield with a layer of galvanized copper on the backside. A lower panel of Fig. 2 shows a CAD drawing of the heat shield with the installed ICE detector. The heat shield is shown in semi-transparent pink, and the four housings with ICE probes are shown in gray. 50 Ω Kapton-insulated coaxial cables around 2 m long each are guided to the flange inside oxygen-free copper tubes shown in brown.

One of the key parameters for the installation of the ICE probes is their maximum allowed temperature. In our case, the limiting factor is the Kapton-isolated cable with the maximum operation temperature of 250 °C. We made a conservative estimate of the temperature distribution on the heat shield in the maximum heating power steady-state scenario as a function of radius by solving the 1D heat transfer equation in polar coordinates. The conservative calculations showed that the maximum temperature is expected on the edge and it will not exceed 180 °C, 70° below the maximum allowed temperature. The calculation results are shown in Fig. 3.

The diagnostic should be able to resolve poloidal and toroidal wavenumbers of the detected ICE. This is done by measuring the relative phase shift in the signal in the respective pair of probes, arranged to measure either poloidal or toroidal perturbations of the magnetic field. Therefore, it is important to know what the instrument-induced relative phase shift is as a function of frequency. Although all four detectors have the same design, the lengths of coaxial cables connecting the probes with the vacuum feedthroughs vary slightly. Capacitive effects of the contacts, where coaxial cables are clamped to the inductors, may also differ from probe to probe. The relative phase shift is measured for frequencies of 10–60 MHz for the pairs of probes 1–3 arranged poloidally and 2–4 arranged toroidally. A SUMIDA inductor, the same as used in the probes, is connected through a matched line to the generator and inductively coupled to each of the four probes. The measurement scheme is shown in Fig. 4. The phase differences between the two probes of a pair are then obtained by

$$(\phi_g - \phi_j) - (\phi_g - \phi_i) = \phi_i - \phi_j = \Delta\phi_{ij}. \quad (1)$$

The phase ϕ_g of the generator cancels and the desired phase difference $\Delta\phi_{ij}$ between the two probes of a pair is obtained, one phase difference for the toroidal pair and one for the poloidal pair. The resulting subtraction is shown in Fig. 5. If the phase difference comes only from the signal delay τ due to different cable lengths inside the copper tubes, we can calculate the corresponding cable length
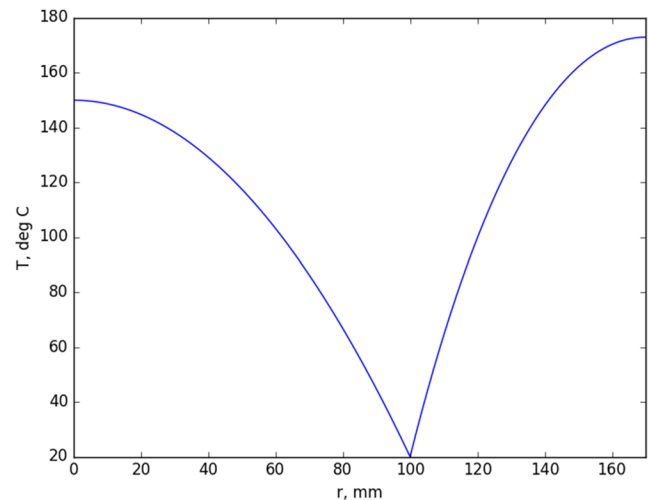

FIG. 3. Distribution of temperature on the CTS heat shield approximated by a disc with a radius of 170 mm and cooling pipe in a circular arrangement with $T_0 = T(r_0) = 20$ °C at r = 100 mm.
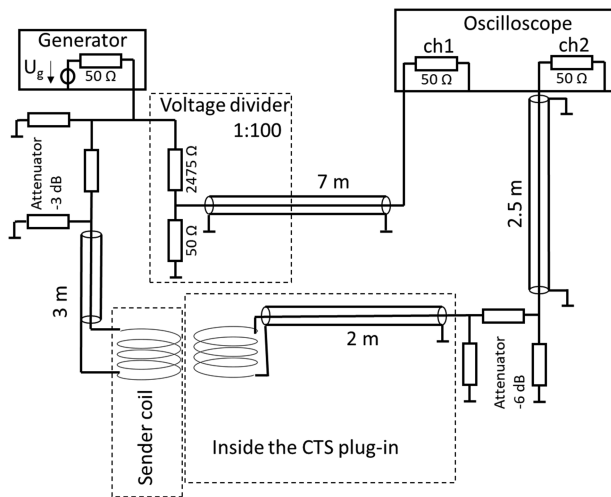
FIG. 4. A schematic showing an experimental setup for the phase–frequency measurements.

difference and check the results for consistency,

$$\Delta\phi_{ij} = 360 \cdot \tau f = 360 \cdot f \frac{\Delta L_{ij} n}{c}. \tag{2}$$

Here, f is the frequency, ΔL_{ij} is the difference in length between cables i and j, n is the relative refraction index, which is ~1.5 for the coaxial cable, and c is the speed of light. We obtain the following length differences: $|\Delta L_{31}| = 13$ cm, $|\Delta L_{42}| = 21$ cm. These agree well with the actual differences in cable lengths. Additionally, a reversed polarity in the connection of the cable in probe 4 is documented. The polarity is reversed with respect to that of probes 1, 2, and 3. It means that having the same input, the output of probe 4 has ~180° phase shift with respect to that of the other three probes.
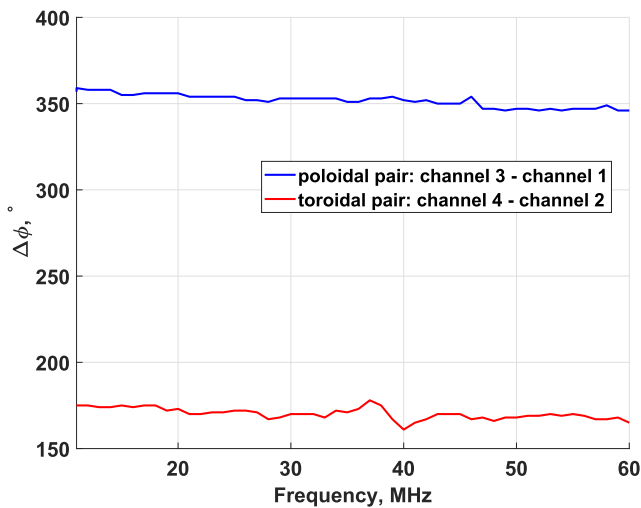

FIG. 5. Phase difference as a function of frequency between probe 3 and probe 1 (blue) and between probe 4 and probe 2 (red).

IV. CONCLUSIONS

The ICE diagnostic was initially installed in 2018 during the commissioning phase of two NBI sources (experimental campaign OP1.2b). The measurements revealed no IC emission, probably due to unfortunate location of the probes inside long and thin immersion tubes for video cameras, where long-wavelength electromagnetic waves are at cutoff. Therefore, for the upcoming experimental campaign, a new location for the ICE probes is found. The detectors are mounted on the backside of the CTS heat shield. This provides the probes with an unobstructed view on the plasma. The conservative analysis of heat distribution on the heat shield shows that, in the harshest scenario with 100 kW/m^2 of plasma radiation, the temperature of the diagnostic will not exceed 180 °C, which is below 250 °C that the Kapton-isolated coaxial cable can withstand.

The diagnostic is prepared for the upcoming experimental campaign in W7-X. It is equipped with four probes measuring changes in the magnetic flux through them. Two measure changes in the toroidal field flux and two in the poloidal field flux. The diagnostic allows measuring signals with frequencies up to 400 MHz and resolves the wave vector of measured radiation in the poloidal and toroidal directions by measuring the relative phase shift of the detected signal in the respective pair of probes. The instrumental function for phase detection is measured.

DATA AVAILABILITY

The data that support the findings of this study are available from the corresponding author upon reasonable request.

REFERENCES

[1]L. G. Askinazi, A. A. Belokurov, D. B. Gin, V. A. Kornev, S. V. Lebedev, A. E. Shevelev, A. S. Tukachinsky, and N. A. Zhubr, Nucl. Fusion **58**, 082003 (2018).

[2]B. Schmidt, M. Salewski, B. Reman, R. O. Dendy, D. Moseev, R. Ochoukov, A. Fasoli, M. Baquero-Ruiz, and H. Järleblad, "Determining 1D fast-ion velocity distribution functions from ion cyclotron emission data using deep neural networks," Rev. Sci. Instrum. (submitted) (2021).

[3]M. Salewski, B. Geiger, D. Moseev, W. W. Heidbrink, A. S. Jacobsen, S. B. Korsholm, F. Leipold, J. Madsen, S. K. Nielsen, J. Rasmussen et al., Plasma Phys. Controlled Fusion **56**, 105005 (2014).

[4]W. W. Heidbrink, Y. Luo, K. H. Burrell, R. W. Harvey, R. I. Pinsker, and E. Ruskov, Plasma Phys. Controlled Fusion **49**, 1457 (2007).

[5]A. S. Jacobsen, M. Salewski, J. Eriksson, G. Ericsson, S. B. Korsholm, F. Leipold, S. K. Nielsen, J. Rasmussen, and M. Stejner, Nucl. Fusion **55**, 053013 (2015).

[6]M. Salewski, M. Nocente, G. Gorini, A. S. Jacobsen, V. G. Kiptily, S. B. Korsholm, F. Leipold, J. Madsen, D. Moseev, S. K. Nielsen et al., Nucl. Fusion **55**, 093029 (2015).

[7]K. G. McClements, R. D'Inca, R. O. Dendy, L. Carbajal, S. C. Chapman, J. W. S. Cook, R. W. Harvey, W. W. Heidbrink, and S. D. Pinches, Nucl. Fusion **55**, 043013 (2015).

[8] R. O. Dendy and K. G. McClements, Plasma Phys. Controlled Fusion **57**, 044002 (2015).

[9] K. E. Thome, D. C. Pace, R. I. Pinsker, M. A. Van Zeeland, W. W. Heidbrink, and M. E. Austin, Nucl. Fusion **59**, 086011 (2019).

[10] M. Ichimura, H. Higaki, S. Kakimoto, Y. Yamaguchi, K. Nemoto, M. Katano, M. Ishikawa, S. Moriyama, and T. Suzuki, Nucl. Fusion **48**, 035012 (2008).

[11] B. Chapman, R. O. Dendy, K. G. McClements, S. C. Chapman, G. S. Yun, S. G. Thatipamula, and M. H. Kim, Nucl. Fusion **57**, 124004 (2017).

[12] R. Ochoukov, R. Bilato, V. Bobkov, B. Chapman, S. C. Chapman, R. O. Dendy, M. Dunne, H. Faugel, M. García-Muñoz, B. Geiger et al., Nucl. Fusion **59**, 014001 (2018).

[13] R. O. Dendy, C. N. Lashmore-Davies, K. G. McClements, and G. A. Cottrell, Phys. Plasmas **1**, 1918 (1994).

[14] R. O. Dendy, K. G. McClements, C. N. Lashmore-Davies, R. Majeski, and S. Cauffman, Phys. Plasmas **1**, 3407 (1994).

[15] K. G. McClements, R. O. Dendy, C. N. Lashmore-Davies, G. A. Cottrell, S. Cauffman, and R. Majeski, Phys. Plasmas **3**, 543 (1996).

[16] T. Fülöp and M. Lisak, Nucl. Fusion **38**, 761 (1998).

[17] R. O. Dendy, C. N. Lashmore-Davies, and K. F. Kam, Phys. Fluids B **5**, 1937 (1993).

[18] R. Ochoukov, K. G. McClements, R. Bilato, V. Bobkov, B. Chapman, S. C. Chapman, R. O. Dendy, M. Dreval, H. Faugel, J.-M. Noterdaeme et al., Nucl. Fusion **59**, 086032 (2019).

[19] N. N. Gorelenkov, New J. Phys. **18**, 105010 (2016).

[20] R. Ochoukov, R. Bilato, V. Bobkov, S. C. Chapman, R. Dendy, M. Dreval, H. Faugel, A. Kappatou, Ye. O. Kazakov, M. Mantsinen et al., Nucl. Fusion **60**, 126043 (2020).

[21] K. Saito, R. Kumazawa, T. Seki, H. Kasahara, G. Nomura, F. Shimpo, H. Igami, M. Isobe, K. Ogawa, K. Toi et al., Plasma Sci. Technol. **15**, 209 (2013).

[22] B. C. G. Reman, R. O. Dendy, T. Akiyama, S. C. Chapman, J. W. S. Cook, H. Igami, S. Inagaki, K. Saito, and G. S. Yun, Nucl. Fusion **59**, 096013 (2019).

[23] L. Liu, R. Ochoukov, K. G. McClements, R. O. Dendy, V. V. Bobkov, M. Weiland, R. Bilato, H. Faugel, D. Moseev, M. Salewski et al., Nucl. Fusion **61**, 026004 (2020).

[24] R. Ochoukov, V. Bobkov, B. Chapman, R. Dendy, M. Dunne, H. Faugel, M. García-Muñoz, B. Geiger, P. Hennequin, K. G. McClements et al., Rev. Sci. Instrum. **89**, 10J101 (2018).

[25] A. Spanier, D. Hartmann, S. Akäslompolo, O. Ford, N. den Harder, B. Heinemann, C. Hopf, R. Kairys, P. McNeely, P. Poloskei et al., Fusion Eng. Des. **163**, 112115 (2021).

[26] M. Preynas, H. P. Laqua, S. Marsen, A. Reintrog, Y. Corre, V. Moncada, and J.-M. Travere, Rev. Sci. Instrum. **86**, 113504 (2015).

[27] R. Ochoukov, V. Bobkov, H. Faugel, H. Fünfgelder, and J.-M. Noterdaeme, Rev. Sci. Instrum. **86**, 115112 (2015).

[28] D. Moseev, M. Stejner, T. Stange, I. Abramovic, H. P. Laqua, S. Marsen, N. Schneider, H. Braune, U. Hoefel, W. Kasparek et al., Rev. Sci. Instrum. **90**, 013503 (2019).